**Advances in Nano Research**, *Vol. 12, No. 6 (2022) 605-616*
https://doi.org/10.12989/anr.2022.12.6.605


# Tuning of the Interparticle interactions in ultrafine ferrihydrite nanoparticles

Yuriy V. Knyazev*[1], Dmitry A. Balaev[1,2], Roman N. Yaroslavtsev[1,2], Aleksandr A. Krasikov[1], Dmitry A. Velikanov[1], Yuriy L. Mikhlin[3], Mikhail N. Volochaev[1], Oleg A. Bayukov[1], Sergei V. Stolyar[1,2] and Rauf S. Iskhakov[1]

[1]*Kirensky Institute of Physics, Federal Research Center KSC SB RAS, Krasnoyarsk, 660036 Russia*
[2]*Siberian Federal University, Krasnoyarsk, 660041 Russia*
[3]*Institute of Chemistry and Chemical Technology, Federal Research Center KSC SB RAS, Krasnoyarsk, 660036 Russia*

(*Received November 16, 2021, Revised March 28, 2022, Accepted March 29, 2022*)

**Abstract.** We prepared two samples of ultrafine ferrihydrite (FH) nanoparticle ensembles of quite a different origin. First is the biosynthesized sample (as a product of the vital activity of bacteria *Klebsiella oxytoca* (hereinafter marked as FH-bact) with a natural organic coating and negligible magnetic interparticle interactions. And the second one is the chemically synthesized ferrihydrite (hereinafter FH-chem) without any coating and high level of the interparticle interactions. The interparticle magnetic interactions have been tuned by modifying the nanoparticle surface in both samples. The coating of the FH-bact sample has been partially removed by annealing at 150°C for 24 h (hereinafter FH-annealed). The FH-chem sample, vice versa, has been coated (1.0 g) with biocompatible polysaccharide (arabinogalactan) in an ultrasonic bath for 10 min (hereinafter FH-coated). The changes in the surface properties of nanoparticles have been controlled by XPS. According to the electron microscopy data, the modification of the nanoparticle surface does not drastically change the particle shape and size. A change in the average nanoparticle size in sample FH-annealed to 3.3 nm relative to the value in the other samples (2.6 nm) has only been observed. The estimated particle coating thickness is about 0.2–0.3 nm for samples FH-bact and FH-coated and 0.1 nm for sample FH-annealed. Mössbauer and magnetization measurements are definitely shown that the drastic change in the blocking temperature is caused by the interparticle interactions. The experimental temperature dependences of the hyperfine field $<H_{hf}>(T)$ for samples FH-bact and FH-coated have not revealed the effect of interparticle interactions. Otherwise, the interparticle interaction energy $E_{int}$ estimated from the $<H_{hf}>(T)$ for samples FH-chem and FH-annealed has been found to be $121k_B$ and $259k_B$, respectively.

**Keywords:** ferrihydrite ultrafine nanoparticles; hyperfine structure; interparticle interactions; iron oxyhydroxide; superparamagnetic relaxation; surface coatings

## 1. Introduction

Hydrous ferric oxide $5Fe_2O_3 \times 8H_2O$ (ferrihydrite) only exists on the nanoscale and is vital for the iron circulation in nature and for microbiology (Kocar *et al*. 2010, Liu *et al*. 2014). Noteworthy is that traces of this mineral were found in water systems not only on the Earth (Schwertmann *et al*. 1999), but also on Mars (Bishop *et al*. 1993, Klingelhöfer *et al*. 2004).

Due to a high rate of surface hydration in ferrihydrite, the particle density in it strongly decreases from the center to the periphery with the formation of a fractal-like morphology (Weidler and Stanjek 1998, Hiemstra 2013, Hiemstra 2018). The rate of hydration is inversely proportional to the particle size (Xu *et al*. 2011, Hiemstra (2013). Since ferrihydrite particles are ultrafine, the mineral has a giant surface area. This property of ferrihydrite can be used for adsorption of organic chemicals (Holsen *et al*. 1991) and heavy metals (Brinza *et al*. 2019, Engel *et al*. 2021).

Moreover, application of the nanomaterials in biomedicine have become a vital task last decades (Chilom *et al*. 2020, Barani *et al*. 2021a, b, c, Sheervalilou *et al*. 2021). Certainly, when choosing materials for biomedical applications, one must be convinced in their chemical and biological harmlessness to the organism and the ease clearance (Sargazi *et al*. 2021, Rahdar *et al*. 2021a, b, Mukhtar *et al*. 2021, Almanghadim *et al*. 2021). Because in living organisms, ferrihydrite is a core of the ferritin complex representing a protein capsule (Papaefthymiou 2010), it is a priori compatible with animal and human cells, which can be used in medicine. Narrow-sized distribution, and high stability of ferrihydrite is of great importance to a rapidly developing area of biomedical applications, such as MRI imaging, specific targeting of the red blood cells, treatment of tumors (Sokolov *et al*. 2018, Lunin *et al*. 2020, Stolyar *et al*. 2018, 2021a, b).

Another parameter, which is important for heating by a magnetic field, is the specific absorption rate (SAR). It was shown that the heating efficiency can be affected by any characteristic that determines the magnetic interactions between nanoparticles (Abbasi *et al*. 2011 Wabler *et al*. 2014). These interactions can be tuned by choosing a synthesis technique (Allia *et al*. 2011, Supraja *et al*. 2016, Rivas Rojas *et al*. 2018, Yusoff *et al*. 2018). Samples of noninteracting or weakly interacting particles can be

*Corresponding author, Ph.D.,
E-mail: yuk@iph.krasn.ru



ISSN: 2287-237X (Print), 2287-2388 (Online)

obtained by coating the latter with inorganic substances, e.g., $SiO_2$ (Rivas Rojas *et al*. 2018, Yakushkin *et al*. 2018) or carbon (Petrov *et al*. 2020). The organic modifiers used are proteins, including dextran (Hong *et al*. 2008), polymer polyethylene glycol (PEG) (Yang *et al*. 2021), and arabinogalactan (Stolyar *et al*. 2018, Kolovskaya *et al*. 2020). The latter is a biologically active substance, so nanoparticles coated with it can be used for its targeted delivery (Groman *et al*. 1996, Yamada 2000). The use of organic coatings can influence the efficiency of application of nanoparticles (Abdolvand *et al*. 2020), since the magnetic properties can be governed via forming additional chemical bonds on the surface or various aggregates (Kamble *et al*. 2014), which is characteristic especially of ferrihydrite, which has a high surface activity (Hiemstra 2018, Stolyar *et al*. 2018, Stolyar *et al*. 2021b).

The interparticle interactions can be enhanced by drying, as was demonstrated on α-$Fe_2O_3$ hematite nanoparticles (Mørup *et al*. 2007). At the same time, the experiments conducted on uncoated antiferromagnetic nanoparticle systems showed that aggregation can drastically change the magnetodynamics in them. For example, the blocking temperature, at which particles become superparamagnetic, can increase by more than 100 K (Hansen *et al*. 2000, Bødker *et al*. 2000, Frandsen *et al*. 2003). The parameter related to the blocking temperature of superparamagnetic (SPM) particles is the magnetic moment relaxation time, which generally obeys the Néel–Braun dependence

$$\tau = \tau_0 \exp\left(\frac{K_{eff}V}{k_BT}\right) \quad (1)$$

Here, $K_{\text{eff}}$ is the effective magnetic anisotropy constant, $V$ is the particle volume, $\tau$ is the characteristic measuring time, and $\tau_0$ is the characteristic particle relaxation time ranging conventionally within $10^{-13}$–$10^{-9}$ s (Mørup *et al*. 2007). Since the parameter $\tau_0$ can influence the SAR (De la Presa *et al*. 2012), the properties of nanomaterials can be controlled by tuning the $\tau_0$ value.

It is natural that the magnetic moments of antiferromagnetic nanoparticles (several hundred Bohr magnetons) are usually much smaller than those of ferromagnetic and ferrimagnetic nanoparticles. The previous estimation of the dipole–dipole interactions on hematite particles with an average diameter of $\langle d \rangle \sim 20$ nm showed that the energy of only the dipole interactions may appear insufficient to significantly affect the SPM relaxation (Hansen *et al*. 2000). At the same time, it was experimentally shown that the blocking temperature of ultrafine antiferromagnetic nanoparticles significantly changes after switching-on the interparticle interactions (Zhao *et al*. 1996, Kuhn *et al*. 2006, 2022, Papaefthymiou *et al*. 2009). Therefore, in ultrafine antiferromagnetic nanoparticle samples, an essential role can be played not only by the exchange coupling, as was assumed by Mørup *et al*. 2007, but also by the dipolar interactions. Taking into account the strong surface anisotropy of fine particles, one can assumed that the behavior of such particles becomes more sensitive to the dipolar interactions as the particle size decreases.

Using the interparticle magnetic interactions, one, in fact, can control the dipole magnetic field when particles are close to each other or somewhat spatially separated. Thus, one can change the speed of rotation of the particle magnetic moment by selecting a required frequency for each specific application. In biogenic ferrihydrite, nanoparticles have a polysaccharide shell (Knyazev *et al*. 2021) and the effect of the interparticle magnetic interactions is negligible, whereas in chemical ferrihydrite these interactions are significant (Knyazev *et al*. 2022). In this study, in order to modify the magnetic properties of nanostructured ferrihydrite systems, we tuned the interparticle magnetic interactions by two methods. The first method uses artificial coating of chemical ferrihydrite nanoparticles (Knyazev *et al*. 2022) with an arabinogalactan protein and the second method consists in annealing of bacterial ferrihydrite (Balaev *et al*. 2016a, Balaev *et al*. 2016b, Balaev *et al*. 2020).

## 2. Experimental

### *2.1 Synthesis*

The synthetic ferrihydrite samples were obtained chemically as described in (Stolyar *et al*. 2017, Knyazev *et al*. 2022). All chemicals used were of analytical grade and required no further purification. The synthetic ferrihydrite samples were prepared by hydrolysis of iron (III) nitrate. Droplets of the 1M NaOH solution were added to the 100 ml $Fe(NO_3)_3 \cdot 9H_2O$ solution (0.2 M) at a rate of 20 ml/min at room temperature under constant stirring until neutral pH. As a result, a dark brown suspension was formed. The obtained precipitate was washed with deionized water to remove remaining ions and dried at room temperature. The sample was a powder of ferrihydrite nanoparticles. To synthesize arabinogalactan-coated ferrihydrite (sample FH-coated), the suspension after washing was added with 1.0 g of arabinogalactan and sonicated for 10 min (22 kHz, 50 W/cm$^2$).

The bacterial ferrihydrite sample (FH-bact) was synthesized by cultivating *Klebsiella oxytoca* bacteria as in our previous study (Knyazev *et al*. 2021). A part of the sample was annealed at a temperature of 150°C in an air atmosphere for 24 h to partially remove the biogenic polysaccharide coating. The obtained sample is hereinafter referred to as FH-annealed.

### *2.2 Transmission electron microscopy*

The size and phase composition of the nanoparticles were controlled by transmission electron microscopy (TEM) and electron microdiffraction, respectively. The electron microscopy and microdiffraction investigations were carried out on a Hitachi HT7700 transmission electron microscope at an accelerating voltage of 100 kV. Specimens were prepared by shaking the nanoparticle powder in alcohol in an ultrasonic bath and depositing the obtained suspension onto support meshes with a perforated carbon

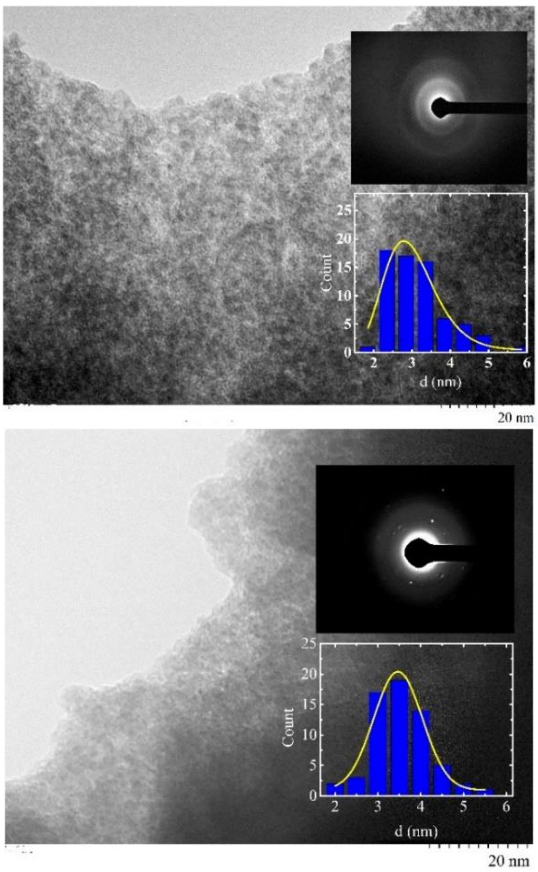


Fig. 1 TEM images for ferrihydrite samples FH-coated and FH-annealed; The lower insets show the calculated particle size distributions (in the bottom); The solid line in the plots corresponds to the processing by the lognormal distribution law; The upper insets show microdiffraction of the samples

coating. The average particle size in the sample was determined using the Scherrer formula. This method takes into account the broadening of diffraction reflections due to size effects. To determine the average particle size, a halfwidth of the first brightest diffraction ring was examined.

The estimation based on the electron microdiffraction data yielded average particle diameters of $<d>$ ~ 2.6 nm and $<d>$ ~ 3.3 nm for samples FH-coated and FH-annealed, respectively. For an ensemble of particles, size histograms were built. The particle size distribution was estimated from microphotographs by conventional computer tools. The histograms are shown in the inset to Fig. 1. The average particle diameters determined from the histograms are $<d>$ ~3.0 nm and $<d>$ ~ 3.45 nm for samples FH-coated and FH-annealed, respectively. These values slightly exceed the Scherrer formula results. This discrepancy is easy to explain. It can be due to the fact that electron microdiffraction was observed directly on a ferrihydrite crystallite, while the physical counting of particles was made from the size visualized in TEM images with allowance for the coating substance. Thus, the discrepancy between the size estimates can be related to the organic coating of the samples.

At the same time, a slight increase in the particle size in sample FH-annealed as compared with sample FH-bact is caused by coarsening of particles during their agglomeration and partial crystallization (Balaev *et al*. 2016a, Balaev *et al*. 2016b, Balaev *et al*. 2020).

The average particle size estimated from the Scherrer formula for sample FH-coated coincides with the value obtained for the chemically synthesized uncoated sample (Knyazev *et al*. 2022). Therefore, the arabinogalactan coating thickness is easy to estimate as a half of the difference between the particle sizes obtained from the Scherrer formula and observed visually. Our estimate for sample FH-coated is ~0.2 nm, which is similar to the value for bacterial ferrihydrite reported in (Knyazev *et al*. 2021), where we already noted the absence of interparticle interactions.

Concerning sample FH-annealed synthesized by annealing of bacterial ferrihydrite, we should note a significant increase in the average particle size as compared with its value in the initial sample. This is confirmed also by the observed diffraction reflections corresponding to the ferrihydrite structure. The resulting discrepancy between the estimated average particle sizes for the annealed sample is ~0.1 nm, which is smaller than for sample FH-coated. Thus, annealing of nanoparticles decreases the organic coating thickness; however, the visual particle size increases, possibly due to aggregation of particles.

In addition, we should pay attention that the particle size distribution for sample FH-coated changed as compared with the original (FH-chem) sample, for which the normal distribution law was observed (Knyazev *et al*. 2022). For sample FH-coated, we have the lognormal distribution law (inset to Fig. 1). However, in sample FH-annealed, the normal distribution is preserved.

### *2.3 X-Ray Photoelectron Spectroscopy (XPS)*

The coating, surface states of iron cations, formation of new chemical bonds, and change of the charge state of surface atoms were controlled by X-ray photoelectron spectroscopy (XPS).

X-ray photoelectron spectra were recorded with a SPECS instrument (Germany) equipped with a PHOIBOS 150 MCD-9 analyzer operating at a pass energy of 20 eV for survey spectra and 10 eV for high-resolution spectra; the X-ray tube was excited by monochromatic Al Kα irradiation (1486.7 eV). The pressure in an analytical chamber was in the range of $10^{-9}$ mbar. The atomic concentrations were determined from the survey spectra. The high-resolution spectra were fitted with the Gaussian–Lorentzian peak profiles after subtraction of the Shirley-type background. The Fe 2p spectra were fitted with several sets of multiplet lines (four narrow peaks and a wider satellite for $Fe^{3+}$cations) (Biesinger *et al*. 2011*)* in the CasaXPS software.

### *2.4 Mössbauer spectroscopy*

Mössbauer spectra of the investigated samples were obtained on an MS-1104Em spectrometer (the Research

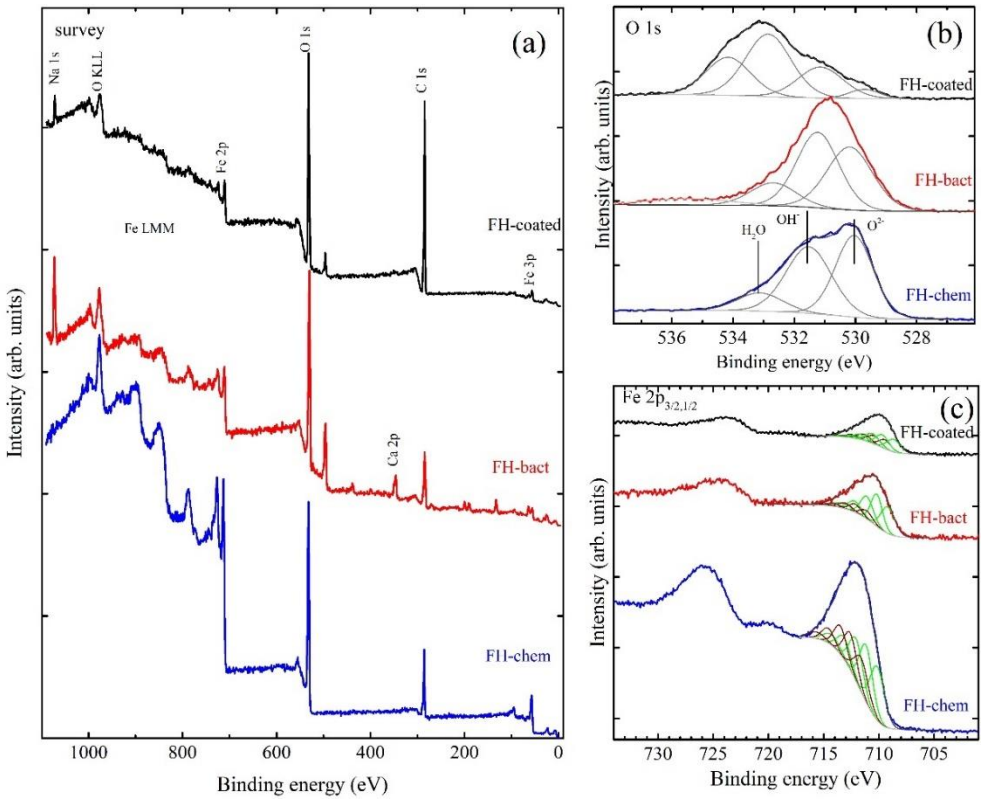


Fig. 2 XPS spectra of ferrihydrite samples; (a) Survey spectra of the samples; (b) Oxygen and (c) iron partial spectra; Two sets of the lines modeling the Fe-2p spectra are shown in different colors

Institute of Physics, Southern Federal University) in the transmission geometry with a $Co^{57}$(Rh) radioactive source in the temperature range of 4–300 K using a CFSG-311-MESS cryostat with a sample in an exchange gas based on a Gifford-McMahon closed cycle cryocooler (Cryotrade Engineering). The modulating signal of motion of the radioactive source was set by a triangular pulse. A sample with a relative thickness of 5 mg/cm$^2$ was placed in a 10-μm-thick aluminum foil and the obtained tablet was pressed and mounted on an insert of a low-temperature cryostat under constant pumping.

Since the difference between the precession angles in an antiferromagnetic nanoparticle is negligible, the number of possible precession states is much smaller than in a ferromagnetic nanoparticle (Mørup *et al*. 2005). Therefore, we determined the relaxation times of the nanoparticle magnetic moments using the model proposed in (Wickman *et al*. 1966). The spectra were processed at the variation of the entire set of hyperfine parameters by the least squares method in the linear approximation.

### *2.5 DC magnetization*

The temperature dependences of the magnetization were measured on a SQUID magnetometer under zero field cooling (ZFC) and field cooling (FC) in the external field range of 1–100 Oe (Velikanov 2013). To perform the magnetic measurements, the investigated powder was fixed in a measuring capsule in paraffin. The magnetic moment data are given in units of emu per powder mass.

## 3. Results

### *3.1 X-Ray photoelectron spectroscopy (XPS)*

The XPS spectra of the samples obtained at 300 K are shown in Fig. 2. The survey spectra (Fig. 2(a)) reveal small sodium and calcium impurities in samples FH-bact and FH-coated. This is indicative of the presence of organic matter in them. A noticeable Ca content in sample FH-bact can be a fingerprint of its organic coating.

The oxygen spectra are decomposed into the $O^{2-}$ lines with a binding energy of ~530 eV, $OH^-$ lines (~531.6 eV), and absorbed water lines (~533 eV), which is consistent with the ferrihydrite spectra presented by Mallet *et al*. (2013). The last two components can contain the oxygen contribution from the carbon-containing coating layer; after the formation of an artificial coating on sample FH-coated, they are noticeably intensified and the $O^{2-}$peak lowers. A ratio of about unity or more (for the coated sample) between the intensities of signals of hydroxide groups and $O^{2-}$ qualitatively agrees with the conclusion about a significant contribution of the hydroxylated surface layer.

The high-resolution spectra of iron are shown in Fig. 2(c). They are in the qualitative agreement with the ferrihydrite spectra presented in Grosvenor *et al*. (2004). In the spectra, the Fe 2p maximum for the main $2p_{3/2}$ level has a binding energy of ~711.2 eV and the broader low-intensity peak at ~720 eV is characteristic of iron oxyhydroxides (Landers *et al*. 2014). A decrease in the total intensity of the lines indicates that the relative iron concentration in the samples

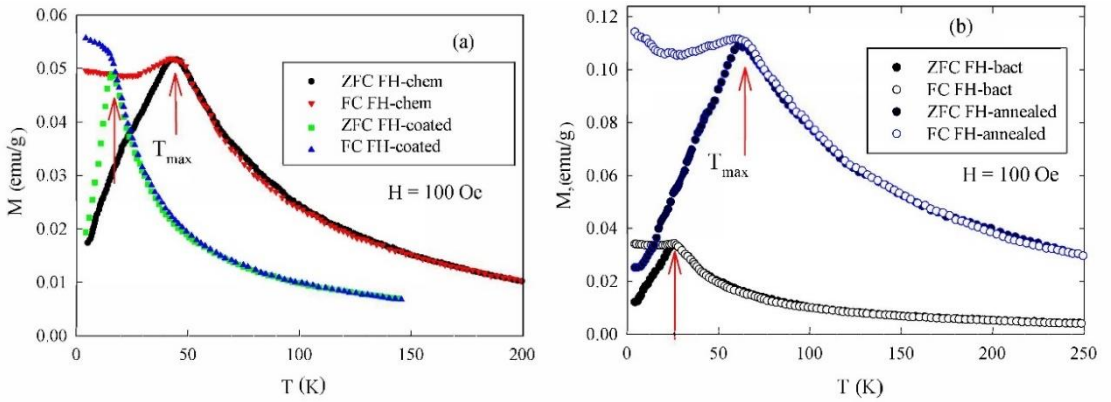


Fig. 3 Temperature dependences of the magnetization of samples (a) FH-chem and FH-coated and (b) FH-bact and FH-annealed at 4–300 K in a magnetic field of 100 Oe. Arrows show the $T_{max}$ values

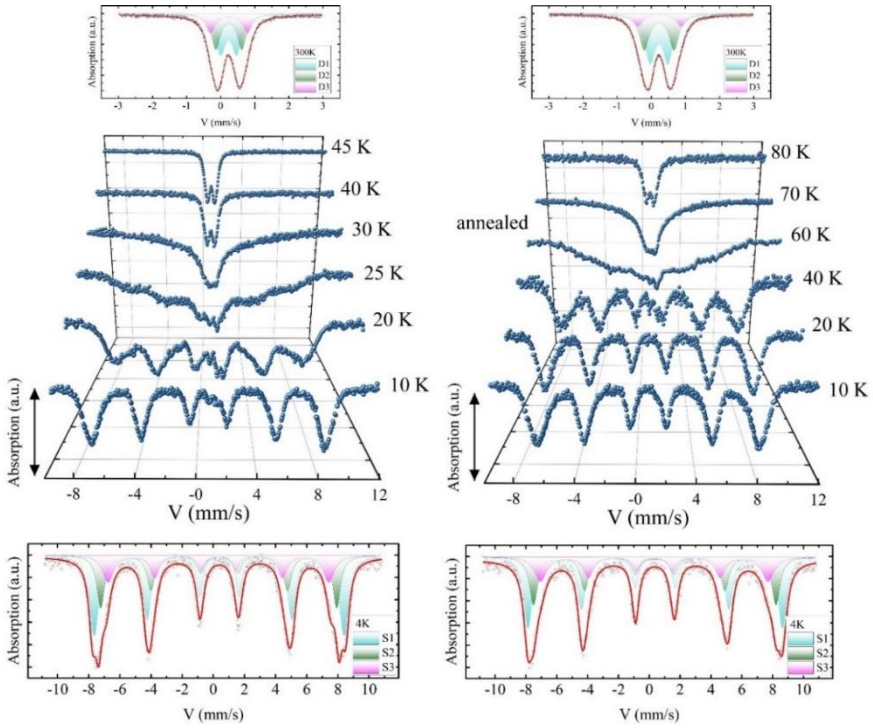


Fig. 4 Mössbauer spectra for samples FH-coated (on the left) and FH-annealed (on the right) in the temperature range of 4–300 K. Spectral components for the samples at 4 and 300 K are shown by shaded areas. The solid line corresponds to the processing data

decreases with the formation of artificial and natural organic coatings of nanoparticles. The highest iron concentration is observed in sample FH-chem and the lowest one, in sample FH-coated with the artificial coating. This is somewhat inconsistent with the estimated coating thickness, which showed that sample FH-bact has a thicker coating than sample FH-coated. However, considering that the molecular weights of the coating substances (organics in the bacteria and arabinogalactan habitat) are different, there is no contradiction here. In the spectra, the Fe $2p_{3/2}$ peak position shifts toward lower binding energies for the coated samples relative to sample FH-chem.

### *3.2 DC magnetization*

Fig. 3 shows the $M(T)$ dependences of the samples obtained in the ZFC mode and in a magnetic field of 100 Oe (FC). Temperature $T_{max}$ corresponding to the maximum magnetization of SPM particles in the dependence is conventionally determined as a magnetic moment blocking temperature. The measurements showed that the numerical values of this temperature are 16 and 44 K for samples FH-coated and FH-chem in Fig. 3(a), respectively. Around $T_{max}$, there is a discrepancy between the $M(T)_{ZFC}$ and $M(T)_{FC}$ dependences, which has the largest value for FH-annealed (Fig. 3(b)). This feature often accompanies the SPM blocking process and is related to the existing particle size distribution (Landers *et al*. 2014, Knyazev *et al*. 2022). The data obtained are indicative of a strong dependence of the $T_{max}$ value on the interparticle interactions.

Note that, in the samples with the surface depleted in an organic coating (FH-annealed and FH-chem), the $T_{max}$ value

Table 1 Mössbauer parameters of sample FH-coated in the temperature range of 4–300 K. IS is the chemical shift relative to α-Fe, $H_{hf}$ is the hyperfine field on iron nuclei, QS is the quadrupole splitting, $W$ is the Mössbauer line FWHM, τ is the calculated magnetic moment relaxation time, and $A$ is the relative site occupancy

| | IS, ±0.005 mm/s | $H_{hf}$, ±3 kOe | QS, mm/s ±0.01 | $W$, ±0.01 mm/s | τ, ns | $A$, ±0.03 a. u. |
|---|---|---|---|---|---|---|
| | | | 300 K | | | |
| 1 | 0.341 | -- | 0.47 | 0.36 | -- | 0.43 |
| 2 | 0.348 | -- | 0.76 | 0.32 | -- | 0.36 |
| 3 | 0.351 | -- | 1.09 | 0.33 | -- | 0.21 |
| | | | 50 K | | | |
| 1 | 0.456 | -- | 0.51 | 0.43 | -- | 0.47 |
| 2 | 0.467 | -- | 0.80 | 0.37 | -- | 0.32 |
| 3 | 0.464 | -- | 1.18 | 0.37 | -- | 0.21 |
| | | | 40 K | | | |
| 1 | 0.476 | -- | 0.42 | 0.39 | -- | 0.15 |
| 2 | 0.469 | -- | 0.75 | 0.37 | -- | 0.28 |
| 3 | 0.470 | -- | 1.18 | 0.43 | -- | 0.23 |
| 4 | 0.460 | 130 | 0.74 | | 0.040 | 0.34 |
| | | | 30 K | | | |
| 1 | 0.470 | 373 | 0.00 | -- | 0.32 | 0.85 |
| 2 | 0.453 | -- | 1.04 | -- | -- | 0.15 |
| | | | 25 K | | | |
| 1 | 0.505 | 412 | 0.01 | -- | 10.0 | 0.54 |
| 2 | 0.496 | 258 | 0.65 | -- | 12.0 | 0.29 |
| 3 | 0.469 | 152 | 1.05 | -- | 7.30 | 0.17 |
| | | | 20 K | | | |
| 1 | 0.471 | 443 | 0.00 | -- | 23.0 | 0.46 |
| 2 | 0.478 | 368 | -0.05 | -- | 26.0 | 0.30 |
| 3 | 0.492 | 256 | 0.00 | -- | 20.0 | 0.24 |
| | | | 10 K | | | |
| 1 | 0.486 | 491 | -0.02 | -- | 52.0 | 0.37 |
| 2 | 0.474 | 461 | -0.07 | -- | 50.0 | 0.36 |
| 3 | 0.499 | 421 | -0.05 | -- | 34.0 | 0.27 |
| | | | 4 K | | | |
| 1 | 0.485 | 499 | -0.04 | -- | 48.0 | 0.51 |
| 2 | 0.466 | 471 | -0.07 | -- | 58.0 | 0.28 |
| 3 | 0.497 | 441 | -0.02 | -- | 53.0 | 0.21 |

is several times higher than the blocking temperature of the samples with the thicker coating. Below this temperature, the FC magnetization of synthetic sample FH-chem has a weak minimum, which is also related to the collective effects caused by the interparticle interactions (Knyazev et .al 2022). A similar regularity can be followed in the dependence for annealed bacterial sample FH-annealed. Synthetic sample FH-coated with arabinogalactan on its surface has no such a characteristic minimum in its FC-magnetization curve, which means that the collective effects vanish. Note that this $M(T)$ behavior qualitatively corresponds to the temperature dependence of the magnetization of bacterial sample FH-bact.

### *3.3 Mössbauer spectroscopy*

Fig. 4 presents the Mössbauer spectra of ferrihydrite samples FH-coated and FH-annealed. According to the mathematical processing data (Tables 1-2), at 300 K, the spectral parameters correspond to the previously obtained data for ferrihydrite, both biogenic and chemical (Zhao *et al*. 1996, Papaefthymiou *et al*. 2009, Stolyar *et al*. 2018, Knyazev *et al*. 2021, 2022). The results of mathematical processing of the spectra for all the samples are consistent (Tables 1 and 2). According to the spectral processing data, iron cations are only in the $3^+$ charge state, which does not change with decreasing temperature. The spectra reveal

Table 2 Mössbauer parameters of sample FH-annealed in the temperature range of 4–300 K. IS is the chemical shift relative to α-Fe, $H_{hf}$ is the hyperfine field on iron nuclei, QS is the quadrupole splitting, *W* is the Mössbauer line FWHM, τ is the calculated magnetic moment relaxation time, and *A* is the relative site occupancy

| | IS, ±0.005 mm/s | $H_{hf}$, ±3 kOe | QS, mm/s ±0.01 | *W*, ±0.01 mm/s | τ, ns | *A*, ±0.03 a. u. |
|---|---|---|---|---|---|---|
| | | | 300 K | | | |
| 1 | 0.336 | -- | 0.52 | 0.37 | -- | 0.51 |
| 2 | 0.338 | -- | 0.87 | 0.35 | -- | 0.37 |
| 3 | 0.347 | -- | 1.27 | 0.33 | -- | 0.13 |
| | | | 100 K | | | |
| 1 | 0.435 | -- | 0.53 | 0.48 | -- | 0.56 |
| 2 | 0.439 | -- | 0.92 | 0.38 | -- | 0.31 |
| 3 | 0.421 | -- | 1.35 | 0.33 | -- | 0.13 |
| | | | 70 K | | | |
| 1 | 0.380 | 133 | 0.00 | -- | 1.00 | 0.56 |
| 2 | 0.433 | 230 | 0.00 | -- | 7.20 | 0.18 |
| 3 | 0.451 | -- | 0.83 | 0.88 | | 0.26 |
| | | | 60 K | | | |
| 1 | 0.567 | 218 | 0.00 | -- | 3.10 | 0.85 |
| 2 | 0.572 | 368 | 0.00 | -- | 19.0 | 0.13 |
| | | | 40 K | | | |
| 1 | 0.479 | 463 | 0.00 | -- | 35.0 | 0.40 |
| 2 | 0.459 | 417 | -0.11 | -- | 31.0 | 0.35 |
| 3 | 0.542 | 343 | -0.01 | -- | 16.0 | 0.23 |
| | | | 30 K | | | |
| 1 | 0.478 | 485 | 0.01 | -- | 44.0 | 0.43 |
| 2 | 0.457 | 451 | -0.03 | -- | 42.0 | 0.34 |
| 3 | 0.473 | 404 | 0.00 | -- | 30.0 | 0.21 |
| | | | 20 K | | | |
| 1 | 0.468 | 499 | 0.01 | -- | 52.0 | 0.44 |
| 2 | 0.454 | 471 | -0.05 | -- | 52.0 | 0.33 |
| 3 | 0.482 | 433 | 0.00 | -- | 39.0 | 0.21 |
| | | | 15 K | | | |
| 1 | 0.484 | 505 | 0.01 | -- | 53.0 | 0.46 |
| 2 | 0.454 | 478 | -0.08 | -- | 54.0 | 0.34 |
| 3 | 0.481 | 442 | 0.00 | -- | 46.0 | 0.19 |
| | | | 10 K | | | |
| 1 | 0.482 | 511 | 0.05 | -- | 51.0 | 0.45 |
| 2 | 0.466 | 486 | -0.04 | -- | 57.0 | 0.31 |
| 3 | 0.474 | 455 | 0.00 | -- | 42.0 | 0.23 |
| | | | 4 K | | | |
| 1 | 0.489 | 515 | 0.01 | -- | 51.0 | 0.461 |
| 2 | 0.464 | 491 | -0.01 | -- | 60.0 | 0.306 |
| 3 | 0.474 | 459 | 0.01 | -- | 45.0 | 0.219 |

three characteristic iron sites in the octahedral environment, which is typical of ferrihydrite (Berquó *et al*. 2009, Stolyar *et al*. 2018). The occupancy of these sites decreases with an increase in the quadrupole splitting (local distortions) and the ratio between the occupancies of these sites remains invariable over the entire temperature range, except for the region around the blocking temperature, where the iron sites cannot be separated because of the relaxation shape of the spectra.

Since the blocking temperature of nanoparticles strongly

depends on their size, it is conventionally determined at the equal areas of the magnetically split (sextet) and quadrupole (doublet) parts of the spectrum (Mørup 1987). Then, it corresponds to blocking of the particles corresponding to the maximum in the particle size distribution. This method, however, is not always applicable. It can be limited by a broad distribution of hyperfine fields (Guyodo *et al*. 2006). This phenomenon is directly related to the relaxation character of the spectra in this region, which is observed for strongly interacting particles (Kuhn *et al*. 2006, Mørup *et al*. 2007). This complexity is typical of both samples FH-coated and FH-annealed and was observed previously in the FH-chem system (Knyazev *et al*. 2021). Such a behavior is induced by the interparticle interactions in a nanoparticle ensemble.

According to the Mössbauer spectroscopy data, the blocking temperature of sample FH-coated is $T_B$ ~ 45 K. This is twice as low as in initial artificially synthesized uncoated sample FH-chem ($T_B$ ~ 90 K) (Knyazev *et al*. 2021). Moreover, a value of $T_B$ ~ 45 K is similar to that observed in biogenic sample FH-bact ($T_B$ ~ 30 K) (Knyazev *et al*. 2022). In this case, annealing of the bacterial sample strongly increases the blocking temperature: this parameter for sample FH-annealed is $T_B$ ~ 85 K. Thus, the enhancement of the interparticle interactions leads to a significant increase in the blocking temperature (Knyazev *et al*. 2022).

Furthermore, it can be noted that weakening of the interparticle interactions causes a significant narrowing of the temperature range of existence of the relaxation region in sample FH-coated, which is fairly narrow (20–40 K). In addition, we should note a narrow (30–40 K) region of existence of the doublet and sextet. However, for the biogenic sample, this behavior is observed during the entire magnetic moment blocking process (Knyazev *et al*. 2022). We attribute the residual relaxation behavior of the spectra to the possible formation of coarser nanoparticles or coated agglomerates of fine particles, which was noted in the TEM data. Such particles can induce much stronger magnetic fields around themselves due to an increase in the uncompensated magnetic moment.

The opposite situation is observed upon annealing of bacterial ferrihydrite. For sample FH-annealed, the relaxation region existing in the range of 40–80 K significantly expands (Fig. 4). This is comparable with our results for sample FH-chem reported in Knyazev *et al*. 2022. In addition, note a strong change in the relaxation time $\tau_0$ for the samples with different degrees of coating. Since no crucial changes in the particle size distribution were observed, this is just the manifestation of the interparticle interactions.

## 4. Discussion

The data obtained for ferrihydrite sample FH-coated are in qualitative agreement with the results reported by Berquó *et al*. 2009, where the change in the shape of the Mössbauer spectra after coating of ferrihydrite nanoparticles with organic substances was also discussed. The SPM relaxation times given in Tables 1-2 clearly demonstrate that the nanoparticle coating thickness directly affects the magnetic moment rotation speed, which has prospects for application.

Let us turn to the temperature dependence of the average hyperfine field $\langle H_{\rm hf}\rangle(T)$ shown in Fig. 5 for ensembles of ferrihydrite particles with different degrees of interparticle interactions. One can clearly see the qualitative change in the $\langle H_{\rm hf}\rangle(T)$ dependence at the modification of the nanoparticle surface. For ensembles of ferrihydrite particles with the natural (FH-bact) and artificial (FH-coated) coatings, the hyperfine fields behave almost identically. A slight discrepancy can be attributed to a certain fraction of the residual interparticle interactions in sample FH-coated. A similar situation is observed for the second pair of nanoparticle systems. Here, we can note that the annealing of the bacterial sample caused even stronger interactions than in sample FH-chem.

In the case of samples FH-chem and FH-annealed, there is a linear portion in the $\langle H_{\rm hf}\rangle(T)$ dependence in the range of 4–40 K, which is especially pronounced for the annealed sample. Above 40 K, the Mössbauer spectra have a relaxation form. This behavior of the temperature dependence of the hyperfine field is typical of interacting particles and can be mathematically described, taking into account the interparticle interaction energy $E_{\rm int}$, as (Frandsen *et al*. 2005, Kuhn *et al*. 2006, Mørup *et al*. 2007)

$$\left\langle H_{hf}\right\rangle(T)=\left\langle H_{hf\,0}\right\rangle\left(1-\frac{k_BT}{2K_{eff}V+E_{\rm int}}\right) \qquad (2)$$

Here, $H_{\rm hf0}$ is the hyperfine field at the minimum temperature. Since the FH-chem and FH-annealed particle sizes are very similar, it can be assumed that the anisotropy constants $K_{\rm eff}$ in these nanoparticle ensembles are also similar. After linearizing the low-temperature portions in Fig. 5, we determined the numerical values of the interparticle interaction energy with allowance for the inclination angle. The $E_{\rm int}$ values for samples FH-chem and FH-annealed are $121k_B$ and $259k_B$, respectively. It is noteworthy that these values are smaller than those for hematite particles with an average size of 8 nm (according to the data reported by Mørup *et al*. 2007) by almost an order of magnitude. We attribute the large difference to the ultra-small particle size in the ensembles under study.

If in Eq. (2) we omit the term $E_{\rm int}$, then the temperature dependence of the hyperfine field for noninteracting particles will be obtained, which is shown in Fig. 5 by the dashed line. This line can be taken as an approximation of the low-temperature behavior of the hyperfine field for samples FH-bact and FH-coated. The best agreement is observed for sample FH-bact; the minor discrepancy for sample FH-coated can be caused by the residual interparticle interactions.

The calculated relaxation times $\tau$ for FH-annealed and FH-chem nanoparticles as a function of temperature are shown by symbols in Fig. 6. Since the time window for the Mössbauer spectroscopy resolution lies within $10^{-8}$–$10^{-10}$ s, the $\tau$ values beyond this range are not analyzed. According to the Wickman model (Wickman *et al*. 1966), at $\tau > 10^{-8}$ s, the shape of the spectrum remains invariable and only the spectral linewidth changes, which becomes smaller than the natural linewidth of nuclear transitions in $^{57}$Fe in this range

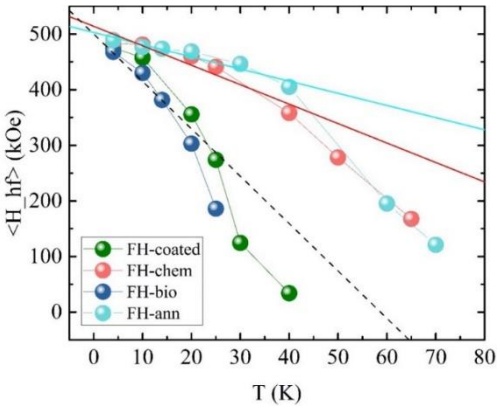


Fig. 5 Temperature dependence of the average hyperfine field for the ferrihydrite samples; The data for samples FH-chem and FH-bact are borrowed from (Knyazev *et al.* 2021) and (Knyazev *et al*. 2022), respectively; The solid lines show linearization by Eq. (2); The dashed line shows the $<H_{hf}>(T)$ dependence with disregard of the interparticle interactions

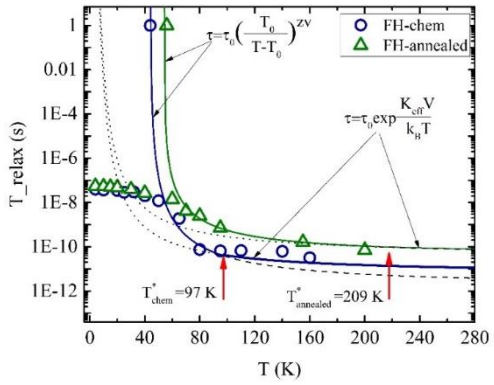


Fig. 6 Temperature dependence of the SPM relaxation time of the magnetic moment for samples FH-annealed and FH-chem obtained from the Mössbauer and dc-magnetization measurement data; Arrows show the temperatures below which the interparticle interactions occur. Dotted and dashed lines show the result of fitting by Eqs. (1) and (3), respectively

and τ loses its physical meaning. In addition, taking into account the characteristic time of the magnetic measurement (1–10 s), the relaxation time at $T_{max}$ (Fig. 3) was taken to be 1 s.

It is well-known that the relaxation time in ensembles of interacting nanoparticles diverges as in the spin glass upon cooling the sample to the phase transition temperature (Fiorani *et al*. 1999, López-Ruiz *et al*. 2010, Morup *et al*. 2010); therefore, to fit the $\tau(T)$ dependence, we used the expression obtained from the scaling law (Morup *et al*. 2010)

$$\tau = \tau_0 \left( \frac{T_0}{T - T_0} \right)^{zv} \qquad (3)$$

Here, the exponent *zv* for systems of interacting particles is 4–12 and $T_0$ is the magnetic moment freezing point. According to the above-obtained estimates of the magnetic interparticle interaction energy, it can be assumed that, in the high-temperature region, Eq. (3) will be in poor agreement with the τ values determined in the Mössbauer experiment. Therefore, to approximate the obtained dependence, we also used Eq. (1), which describes the change in the SPM relaxation time for the nanoparticle magnetic moments in an ensemble without interactions. Figure 6 shows the result of processing of the obtained data. It can be seen that both samples follow the same regularity: above the temperature *T** (arrows in Fig. 6), Eq. (1) better describes the $\tau(T)$ dependence. At the same time, below *T**, due to the interactions between nanoparticles, the $\tau(T)$ dependence exhibits a sharper and more pronounced growth than Neel–Brown dependence (1) and obeys Eq. (3). The latter is consistent with the previous results for ferrimagnetic nanoparticles (López-Ruiz *et al*. 2010, Morup *et al*. 2010). Note that, for sample FH-annealed, the exponent is *zv* = 6, which is significantly higher than for sample FH-chem (*zv* = 4). The numerical *T** values for these nanoparticle ensembles are consistent with the estimated interparticle interaction energies.

## 5. Conclusions

We note that the technological route for the synthesis of artificial or biological ferrihydrite does not significantly affect the manifestation of collective effects induced by the interparticle interactions. In the nanomaterial obtained by both methods, these interactions can be finely tuned by modifying the nanoparticle surface. The surface modification of ultrafine ferrihydrite nanoparticles performed in this study showed that the surface coating strongly affects their magnetic characteristics. This phenomenon is directly related to tuning of the magnetic interparticle interactions. Switching-on the interparticle interactions upon annealing of the bacterial nanoparticle ensemble (FH-annealed) increased the blocking temperature to 85 K, according to the Mössbauer spectroscopy data (56 K, according to the magnetic measurement data). This value corresponds to a Mössbauer blocking temperature of 95 K ($T_{max}$ = 44 K, according to the magnetization data) for initial synthetic ferrihydrite sample FH-chem. On the other hand, the artificial coating eliminates almost completely the interactions between particles and reduces the blocking temperature in sample FH-coated to 30 K, according to the Mössbauer spectroscopy data (16 K, according to the magnetic measurement data).

The interparticle interaction energy $E_{int}$ for samples FH-annealed and FH-chem was estimated from the $<H_{hf}>(T)$ dependence; numerical values of 121 and 259 K, respectively, were obtained. The Mössbauer spectroscopy data in the range of 4–300 K showed that a change in the thickness of the coating of ultrafine ferrihydrite nanoparticles significantly affects the SPM relaxation. The obtained temperature dependences of the relaxation times for the samples with the interparticle interactions (FH-annealed and FH-chem) qualitatively confirmed the estimated interparticle interaction energy. Thus, it was shown that tuning of the interparticle interactions by modifying the coating of antiferromagnetic ferrihydrite

nanoparticles is a promising technique for obtaining the required magnetic properties of nanoparticles.

To sum up, it is evident that the magnetic interparticle interactions in ferrihydrite nanoparticle ensembles may be easily tuned by modifying the nanoparticle surface. Moreover, such phenomenon does not depend on the origin of the matter (bio- or chemically synthesized). Furthermore, we showed that magnetic interparticle interactions drastically change magnetic behavior of the nanoparticle ensembles.

## Acknowledgments

The electron microscopy, XPS, and Mössbauer spectroscopy studies were carried out on the equipment of the Krasnoyarsk Territorial Center for Collective Use, Krasnoyarsk Scientific Center, Siberian Branch of the Russian Academy of Sciences.

## Funding

This study was supported by the Russian Science Foundation, project no. 21-72-00025 “Tuning the Magnetic Properties of Ultrafine Biocompatible Ferrihydrite Nanoparticles through Interparticle Interactions” (https://rscf.ru/project/21-72-00025/).

## References

Abbasi, A.Z., Gutiérrez, L., del Mercato, L.L., Herranz, F., Chubykalo-Fesenko, O., Veintemillas-Verdaguer, S., Parak, W.J., Puerto Morales, M, González, J.M, Hernando, A and de la Presa, P. (2011), “Magnetic capsules for NMR imaging: Effect of magnetic nanoparticles spatial distribution and aggregation”, *J. Phys. Chem. C*, **115**(14), 6257-6264. https://doi.org/10.1021/jp1118234.

Abdolvand, E., Farzinpour, A. and Vaziry, A. (2020), “Effects of supplementation cysteine-coated $Fe_3O_4$ nanoparticles compared to $FeSO_4$, on reproductive performance in male quail”, *Adv. Nano Res.*, **9**(1), 15-24. https://doi.org/10.12989/anr.2020.9.1.015

Almanghadim, H.G., Nourollahzadeh, Z., Khademi, N.S., Tezerjani, M.D., Sehrig, F.Z., Estelami, N., Shirvaliloo, M., Sheervalilou, R. and Sargazi, S. (2021), “Application of nanoparticles in cancer therapy with an emphasis on cell cycle”, *Cell Biol. Int.*, **45**(10), 1989-1998. https://doi.org/10.1002/cbin.11658.

Balaev, D.A., Krasikov, A.A., Dubrovskiy, A.A., Popkov, S.I., Stolyar, S.V., Bayukov, O.A., Iskhakov, R.S., Ladygina, V.P., Yaroslavtsev, R.N. (2016a), “Magnetic properties of heat treated bacterial ferrihydrite nanoparticles”, *J. Magn. Magn. Mater.*, **410**, 171-180. https://doi.org/10.1016/j.jmmm.2016.02.059.

Balaev, D.A., Krasikov, A.A., Stolyar, S.V., Iskhakov, R.S., Ladygina, V.P., Yaroslavtsev, R.N., Bayukov, O.A., Vorotynov, A.M., Volochaev, M.N. and Dubrovskiy, A.A. (2016b), “Change in the magnetic properties of nanoferrihydrite with an increase in the volume of nanoparticles during low-temperature annealing”, *Phys. Solid State*, **58**(9), 1782-1791. https://doi.org/10.1134/s1063783416090092.

Balaev, D.A., Krasikov, A.A., Balaev, A.D., Stolyar, S.V., Ladygina, V.P. and Iskhakov, R.S. (2020), “Features of relaxation of the remanent magnetization of antiferromagnetic nanoparticles by the example of ferrihydrite”, *Phys. Solid State*, **62**(7), 1172-1178. https://doi.org/10.1134/s1063783420070033.

Barani, M., Zeeshan, M., Kalantar-Neyestanaki, D., Farooq, M.A., Rahdar, A., Jha, N.K., Sargazi, S., Gupta, P.K. and Thakur, V. K. (2021a), “Nanomaterials in the management of gram-negative bacterial infections”, *Nanomaterials*, **11**(10), 2535. https://doi.org/10.3390/nano11102535.

Barani, M., Sargazi, S., Mohammadzadeh, V., Rahdar, A., Pandey, S., Jha, N.K., Gupta, P.K. and Thakur, V.K. (2021b), “Theranostic advances of bionanomaterials against gestational diabetes mellitus: A preliminary review”, *J. Funct. Biomater.*, **12**(4), 54. https://doi.org/10.3390/JFB12040054.

Barani, M., Reza Hajinezhad, M., Sargazi, S., Zeeshan, M., Rahdar, A., Pandey, S., Khatami, M. and Zargari, F. (2021c), “Simulation, in vitro and in vivo cytotoxicity assessments of methotrexate-loaded ph-responsive nanocarriers”, *Polymers*, **13**(18), 3153. https://doi.org/10.3390/polym13183153.

Berquó, T.S., Erbs, J.J., Lindquist, A., Penn, R.L. and Banerjee, S.K. (2009), “Effects of magnetic interactions in antiferro-magnetic ferrihydrite particles”, *J. Phys. Condens. Mat.*, **21**(17), 176005. https://doi.org/10.1088/0953-8984/21/17/176005.

Biesinger, M.C., Payne, B.P., Grosvenor, A.P., Lau, L.W.M., Gerson, A.R. and Smart, R.S.C. (2011), “Resolving surface chemical states in XPS analysis of first row transition metals, oxides and hydroxides: Cr, Mn, Fe, Co and Ni”, *Appl. Surf. Sci.*, **257**(7), 2717-2730. https://doi.org/10.1016/j.apsusc.2010.10.051.

Bishop, J.L., Pieters, C. and Burns, R.G. (1993), “Reflectance and Mössbauer spectroscopy of ferrihydrite-montmorillonite assemblages as Mars soil analog materials”, *Geochim. Cosmochim. Acta*, **57(**19**)**, 4583-4595. https://doi.org/10.1016/0016-7037(93)90184-x.

Bødker, F., Hansen, M.F., Koch, C.B. and Mørup, S. (2000), “Particle interaction effects in antiferromagnetic NiO nanoparticles””, *J. Magn. Magn. Mater.*, **221**(1-2), 32-36. https://doi.org/10.1016/S0304-8853(00)00392-9.

Brinza, L., Vu, H.P., Neamtu, M. and Benning, L.G. (2019), “Experimental and simulation results of the adsorption of Mo and V onto ferrihydrite”, *Sci. Rep.*, **9(**1**),** 1-12. https://doi.org/10.1038/s41598-018-37875-y.

Chilom, C.G., Zorilă, B., Bacalum, M., Bălăşoiu, M., Yaroslavtsev, R., Stolyar, S. V. and Tyutyunnicov S. (2020), “Ferrihydrite nanoparticles interaction with model lipid membranes”, *Chem. Phys. Liq.*, **226**, 104851. https://doi.org/10.1016/j.chemphyslip.2019.104851.

De la Presa, P., Luengo, Y., Multigner, M., Costo, R., Morales, M. P., Rivero, G. and Hernando, A. (2012), “Study of heating efficiency as a function of concentration, size and applied field in $\gamma$-$Fe_2O_3$ nanoparticles”, *J. Phys. Chem. C*, **116**(48), 25602-25610. https://doi.org/10.1021/jp310771p.

Engel, M., Lezama Pacheco, J.S., Noël, V., Boye, K. and Fendorf, S. (2021), “Organic compounds alter the preference and rates of heavy metal adsorption on ferrihydrite”, *Sci. Total Environ.*, **750**, 141485. https://doi.org/10.1016/j.scitotenv.2020.1414.

Frandsen, C. and Mørup, S. (2003), “Inter-particle interactions in composites of antiferromagnetic nanoparticles”, *J. Magn. Magn. Mater.*, **266**(1-2), 36-48. https://doi.org/10.1016/S0304-8853(03)00453-0.

Fiorani, D., Dormann, J.L., Cherkaoui, R., Tronc, E., Lucari, F., D’Orazio, F., Spinu, L., Nogues, M., Garcia, A., Testa, A. M. (1999), “Collective magnetic state in nanoparticles systems” *J. Magn. Magn. Mater.*, **196**, 143-147. https://doi.org/10.1016/s0304-8853(98)00694-5.

Frandsen, C. and Mørup, S. (2005), “Spin rotation in $\alpha-Fe_2O_3$ nanoparticles by interparticle interactions”, *Phys. Rev. Lett.*, **94**(2), 027202. https://doi.org/10.1103/PhysRevLett.94.027202.

Groman, E.V., Menz, E.T., Enriquez, P.M., Jung, C., Lewis, J.M.

and Josephson, L. (1996), "Delivery of therapeutic agents to receptors using polysaccharides", U.S. Patent No. 5,554,386; Washington, U.S.A.

Grosvenor, A.P., Kobe, B.A., McIntyre, N.S., Tougaard, S. and Lennard, W.N. (2004), "Use of QUASES™/XPS measurements to determine the oxide composition and thickness on an iron substrate', *Surf. Interf. Anal*., **36**(7), 632-639. https://doi.org/10.1002/sia.1842.

Guyodo, Y., Banerjee, S.K., Penn, R.L., Burleson, D., Berquo, T.S., Seda, T. and Solheid, P. (2006), "Magnetic properties of synthetic six-line ferrihydrite nanoparticles", *Phys. Earth Planet. In*., **154**(3-4), 222-233. https://doi.org/10.1016/j.pepi.2005.05.009.

Hansen, M.F., Koch, C.B. and Mørup, S. (2000), "Magnetic dynamics of weakly and strongly interacting hematite nanoparticles", *Phys. Rev. B*, **62**(2), 1124. http://doi.org/10.1103/PhysRevB.62.1124.

Hiemstra, T. (2013), "Surface and mineral structure of ferrihydrite", *Geochim. Cosmochim. Acta*, **105**, 316-325. https://doi.org/10.1016/j.gca.2012.12.002.

Hiemstra, T. (2018), "Surface structure controlling nanoparticle behavior: magnetism of ferrihydrite, magnetite and maghemite", *Environ. Sci*., **5,** 752-764. https://doi.org/10.1039/C7EN01060E.

Holsen, T.M., Taylor, E.R., Seo, Y.C. and Anderson, P.R. (1991), "Removal of sparingly soluble organic chemicals from aqueous solutions with surfactant-coated ferrihydrite", *Environ. Sci. Technol*., **25(9)**, 1585-1589. https://doi.org/10.1021/es00021a009.

Hong, R.Y., Feng, B., Chen, L.L., Liu, G.H., Li, H.Z., Zheng, Y. and Wei, D.G. (2008), "Synthesis, characterization and MRI application of dextran-coated $Fe_3O_4$ magnetic nanoparticles", *Biochem. Eng. J*., **42(3)**, 290-300. https://doi.org/10.1016/j.bej.2008.07.009.

Kamble, V., Kodwani, G., Sridharkrishna, R. and Ankamwar, B. (2014), "Synthesis of anisotropic defective polyaniline/silver nanocomposites", *Adv. Nano Res*., **2**(2), 111-119. https://doi.org/10.12989/anr.2014.2.2.111.

Klingelhöfer, G., Morris, R.V., Bernhardt, B., Schröder, C., Rodionov, D.S., de Souza, P.A., Yen, A., Gellert, R., Evlanov, E.N., Zubkov, B., Foh, J., Bonnes, U., Kankeleit, E., Gütlich, P., Ming, D.W., Renz, F., Wdowiak, T., Squyres, S.W. and Arvidson, R.E. (2004), "Jarosite and hematite at meridiani planum from opportunity's Mössbauer spectrometer", *Science*, **306(**5702**)**, 1740-1745. http://doi.org/10.1126/science.1104653.

Knyazev, Y.V., Balaev, D.A., Stolyar, S.V., Krasikov, A.A., Bayukov, O.A., Volochaev, M.N., Yaroslavtsev, R.N., Ladygina, V.P., Velikanov, D.A. and Iskhakov, R.S. (2022), "Interparticle magnetic interactions in synthetic ferrihydrite: Mössbauer spectroscopy and magnetometry study of the dynamic and static manifestations", *J. Alloy. Compd*., **889**, 161623. https://doi.org/10.1016/j.jallcom.2021.161623.

Knyazev, Y.V., Balaev, D.A., Stolyar, S.V., Bayukov, O.A., Yaroslavtsev, R.N., Ladygina, V.P., Velikanov, D.A. and Iskhakov, R.S. (2020), "Magnetic anisotropy and core-shell structure origin of the biogenic ferrihydrite nanoparticles", *J. Alloy. Compd*., **851**, 156753. https://doi.org/10.1016/j.jallcom.2020.156753.

Kocar, B.D., Borch, T. and Fendorf, S. (2010), "Arsenic repartitioning during biogenic sulfidization and transformation of ferrihydrite", *Geochim. Cosmochim. Acta*, **74(**3**)**, 980-994. http://doi.org/10.1016/j.gca.2009.10.023.

Kolovskaya, O.S., Zamay, T.N., Zamay, G.S., Babkin, V.A., Medvedeva, E.N., Neverova, N.A., Kirichenko, A.K., Zamay, S.S., Lapin, I. N., Morozov, E.V., Sokolov, A.E., Narodov, A.A., Fedorov, D.G., Tomilin, F.N., Zabluda, V.N., Alekhina, Y.., Lukyanenko, K.A., Glazyrin, Y.E., Svetlichnyi, V.A., Berezovski, M.V. and Kichkailo, A.S. (2020), "Aptamer-conjugated superparamagnetic ferroarabinogalactan nanoparticles for targeted magnetodynamic therapy of cancer", *Cancers*, **12(**1**)**, 216. https://doi.org/10.3390/cancers12010216.

Kuhn, L.T., Lefmann, K., Bahl, C.R.H., Ancona, S.N., Lindgård, P.A., Frandsen, C., Madsen, D.E. and Mørup, S. (2006), "Neutron study of magnetic excitations in8−nmα−$Fe_2O_3$ nanoparticles", *Phys. Rev. B*, **74**(18), 184406. https://doi.org/10.1103/physrevb.74.184406.

Landers, J., Stromberg, F., Darbandi, M., Schöppner, C., Keune, W. and Wende, H. (2014), "Correlation of superparamagnetic relaxation with magnetic dipole interaction in capped iron-oxide nanoparticles", *J. Phys. Condens. Mat.*, **27**(2), 026002. https://doi.org/10.1088/0953-8984/27/2/026002.

Liu, H., Li, X., Wang, Y., Yang, X., Zhen, Z., Chen, R., Hou, D. and Wei, Y. (2014), "New insight into the effect of the formation environment of ferrihydrite on its structure and properties", *RSC Adv.*, **4(**22**)**, 11451-11458. http://doi.org/10.1039/c4ra00696h.

López-Ruiz, R., Luis, F., Sesé, J., Bartolomé, J., Deranlot, C. and Petroff, F. (2010), "Zero-temperature spin-glass freezing in self-organized arrays of Co nanoparticles", *Europhys. Lett.*, **89**(6), 67011. https://doi.org/10.1209/0295-5075/89/67011.

Lunin, A.V., Lizunova, A.A., Mochalova, E.N., Yakovtseva, M.N., Cherkasov, V.R., Nikitin, M.P. and Kolychev, E.L. (2020), "Hematite nanoparticles from unexpected reaction of ferrihydrite with concentrated acids for biomedical applications", *Molecules*, **25**(8), 1984. https://doi.org/10.3390/molecules25081984.

Mallet, M., Barthélémy, K., Ruby, C., Renard, A. and Naille, S. (2013), "Investigation of phosphate adsorption onto ferrihydrite by X-ray photoelectron spectroscopy", *J. Colloid Interf. Sci*., **407**, 95-101. https//doi.org/10.1016/j.jcis.2013.06.049.

Mørup, S. (1987), "Mössbauer effect studies of microcrystalline materials", *Mossbauer Spectroscopy Applied To Inorganic Chemistry*, **2**, 89-123.

Mørup, S. and Hansen, B.R. (2005), "Uniform magnetic excitations in nanoparticles", *Phys. Rev. B*, **72**(2), 024418. https://doi.org/10.1103/PhysRevB.72.024418.

Mørup, S., Madsen, D.E., Frandsen, C., Bahl, C.R. and Hansen, M.F. (2007), "Experimental and theoretical studies of nanoparticles of antiferromagnetic materials", *J. Phys. Condens. Mat*., **19**(21), 213202. https://doi.org/10.1088/0953-8984/19/21/213202.

Mørup, S., Hansen, M.F., Frandsen, C. (2010), "Magnetic interactions between nanoparticles", *Beilstein J. Nanotechnol*., **1**, 182-190. https://doi.org/10.3762/bjnano.1.22.

Papaefthymiou, G.C., Devlin, E., Simopoulos, A., Yi, D.K., Riduan, S.N., Lee, S.S. and Ying, J.Y. (2009), "Interparticle interactions in magnetic core/shell nanoarchitectures", *Phys. Rev. B*, **80**(2), 024406. https://doi.org/10.1103/PhysRevB.80.024406.

Mukhtar, M., Sargazi, S., Barani, M., Madry, H., Rahdar, A. and Cucchiarini, M. (2021), "Application of nanotechnology for sensitive detection of low-abundance single-nucleotide variations in genomic DNA: A review", *Nanomaterials*, **11**(6), 1384. https://doi.org/10.3390/nano11061384.

Papaefthymiou, G.C. (2010), "The Mössbauer and magnetic properties of ferritin cores", *Biochim. Biophys. Acta*, **1800(**8**)**, 886-897. https://doi.org/10.1016/j.bbagen.2010.03.018.

Petrov, D., Lin, C.R., Ivantsov, R., Ovchinnikov, S.G., Zharkov, S., Yurkin, G., Velikanov, D.A., Knyazev, Y.V., Molokeev, M.S., Tseng, Y.T., Lin, E.S., Edelman, I.S., Baskakov, A.O., Starchikov, S.S. and Lyubutin, I.S. (2020), "Characterization of the iron oxide phases formed during the synthesis of core-shell FexOy@C nanoparticles modified with Ag", *Nanotechnology*, **31**, 395703. https://doi.org/10.1088/1361-6528/ab9af2.

Rahdar, A., Hajinezhad, M. R., Sargazi, S., Zaboli, M., Barani, M., Baino, F., Bilal, M. and Sanchooli, E. (2021), "Biochemical,

ameliorative and cytotoxic effects of newly synthesized curcumin microemulsions: Evidence from in vitro and in vivo studies", *Nanomaterials*, **11**(3), 817. https://doi.org/10.3390/nano11030817.

Rahdar, A., Hajinezhad, M. R., Barani, M., Sargazi, S., Zaboli, M., Ghazy, E., Baino, F., Cucchiarini, M., Bilal, M. and Pandey, S. (2022), "Pluronic F127/doxorubicin microemulsions: preparation, characterization and toxicity evaluations", *J. Mol. Liq.*, **345**, 117028. https://doi.org/10.1016/j.molliq.2021.117028.

Rivas Rojas, P.C., Tancredi, P., Moscoso Londoño, O., Knobel, M. and Socolovsky, L.M. (2018), "Tuning dipolar magnetic interactions by controlling individual silica coating of iron oxide nanoparticles", *J. Magn. Magn. Mat.*, **451**, 688-696. https://doi.org/10.1016/j.jmmm.2017.11.099.

Sargazi, S., Hajinezhad, M.R., Rahdar, A., Zafar, M.N., Awan, A. and Baino, F. (2021), "Assessment of $SnFe_2O_4$ nanoparticles for potential application in theranostics: Synthesis, characterization, in vitro and in vivo toxicity", *Materials*, **14**(4), 1-19. https://doi.org/10.3390/ma14040825.

Schwertmann, U., Friedl, J. and Stanjek, H. (1999), "From Fe(III) ions to ferrihydrite and then to hematite", *J. Colloid Interf. Sci.*, **209(**1**)**, 215-223. http://doi.org/10.1006/jcis.1998.5899.

Sheervalilou, R., Shirvaliloo, M., Sargazi, S., Shirvalilou, S., Shahraki, O., Pilehvar-Soltanahmadi, Y., Sarhadi, A., Nazarlou, Z., Ghaznavi, H. and Khoei, S. (2021), "Application of nanobiotechnology for early diagnosis of SARS-CoV-2 infection in the COVID-19 pandemic", *Appl. Microbiol. Biotechnol.*, **105**(7), 2615-2624. https://doi.org/10.1007/s00253-021-11197-y.

Sokolov, I. L., Cherkasov, V. R., Vasilyeva, A. V., Bragina, V. A. and Nikitin, M. P. (2018), "Paramagnetic Colloidal Ferrihydrite Nanoparticles for MRI Contrasting", *Colloid. Surf. A*, **539,** 46-52. https://doi.org/10.1016/j.colsurfa.2017.11.062

Stolyar, S.V., Yaroslavtsev, R.N., Iskhakov, R.S., Bayukov, O.A., Balaev, D.A., Dubrovskii, A.A., Krasikov A.A., Ladygina, V.P., Vorotynov, A.M., Volochaev, M.N. (2017). "Magnetic and resonance properties of ferrihydrite nanoparticles doped with cobalt", *Phys. Solid State*, **59**(3), 555-563. https://doi.org/10.1134/s1063783417030301.

Stolyar, S.V., Balaev, D.A., Ladygina, V.P., Dubrovskiy, A.A., Krasikov, A.A., Popkov, S.I., Bayukov, O.A., Knyazev, Yu.V., Yaroslavtsev, R.N., Volochaev, M.N., Iskhakov, R.S., Dobretsov, K.G., Morozov, E.V., Falaleev, O.V., Inzhevatkin, E.V., Kolenchukova, O.A. and Chizhova, I.A. (2018), "Bacterial ferrihydrite nanoparticles: preparation, magnetic properties and application in medicine", *J. Supercond. Nov. Magn.*, **31**, 2297. https://doi.org/10.1007/s10948-018-4700-1.

Stolyar, S.V., Kolenchukova, O.A., Boldyreva, A.V., Kudryasheva, N.S., Gerasimova, Y.V., Krasikov, A.A., Yaroslavtsev, R.N., Bayukov, O.A., Ladygina, V.P., Birukova, E.A. (2021a), "Biogenic ferrihydrite nanoparticles: Synthesis, properties in vitro and in vivo testing and the concentration effect", *Biomedicines*, **9**(3), 323. https://doi.org/10.3390/biomedicines9030323.

Stolyar, S.V., Kryukova, O.V., Yaroslavtsev, R.N., Bayukov, O.A., Knyazev, Y.V., Gerasimova, Y.V., Pyankov, V.F., Latyshev, N.V. and Shestakov, N.P. (2021b), "Influence of magnetic nanoparticles on cells of Ehrlich ascites carcinoma", *AIP Adv.*, **11**(1), 015019. https://doi.org/10.1063/9.0000165.

Supraja, N., Tollamadugu, N.V.K.V.P. and Adam, S. (2016), "Phytogenic silver nanoparticles (Alstonia scholaris) incorporated with epoxy coating on PVC materials and their biofilm degradation studies", *Adv. Nano Res.*, **4(**4**)**, 281. https://doi.org/10.12989/anr.2016.4.4.281

Velikanov, D.A. (2013), "Squid magnetometer for investigations of the magnetic properties of materials in the temperature range 4.2-370 K", *Sib. J. Sci. Technol.*, **2**(48), 176.

Wabler, M., Zhu, W., Hedayati, M., Attaluri, A., Zhou, H., Mihalic, J., Geyh, A., DeWeese, T.L., Ivkov, R. and Artemov, D. (2014), "Magnetic resonance imaging contrast of iron oxide nanoparticles developed for hyperthermia is dominated by iron content", *Int. J. Hyperther.*, **30(**3**)**, 192-200. https://doi.org/10.3109/02656736.2014.913321.

Weidler, P.G. and Stanjek, H. (1998), "The effect of dry heating of synthetic 2-line and 6-line ferrihydrite: II. Surface area, porosity and fractal dimension", *Clay Miner.*, **33(2)**, 277-284. https://doi.org/10.1180/000985598545471.

Wickman, H.H., Klein, M.P. and Shirley, D.A. (1966), "Paramagnetic hyperfine structure and relaxation effects in mössbauer spectra: $Fe^{57}$ in ferrichrome", *Phys. Rev.*, **152**(1), 345. https://doi.org/10.1103/PhysRev.152.345.

Xu, W., Hausner, D.B., Harrington, R., Lee, P.L., Strongin, D.R. and Parise, J.B. (2011), "Structural water in ferrihydrite and constraints this provides on possible structure models", *Am. Mineralogist*, **96(4)**, 513-520. https://doi.org/10.2138/am.2011.3460.

Yakushkin, S.S., Balaev, D.A., Dubrovskiy, A.A., Semenov, S.V., Knyazev, Y.V., Bayukov, O.A., Kirillov, V.L., Ivantsov, R.D., Edelman, I.S. and Martyanov, O.N. (2018), "ε-$Fe_2O_3$ nanoparticles embedded in silica xerogel - Magnetic metamaterial", *Ceram. Int.*, **44(**15**)**, 17852-17857. https://doi.org/10.1016/j.ceramint.2018.06.254.

Yamada H. (2000), *Bioactive Arabinogalactan-Proteins and Related Pectic Polysaccharides in Sino-Japanese Herbal Medicines*, in: *Cell and Developmental Biology of Arabinogalactan-Proteins*, Springer, Boston, U.S.A. https://doi.org/10.1007/978-1-4615-4207-0_19.

Yang, Y., Tian, Q., Wu, S., Li, Y., Yang, K., Yan, Y., Shang, L., Li, A., Zhang, L. (2021), "Blue light-triggered Fe2+-release from monodispersed ferrihydrite nanoparticles for cancer iron therapy", *Biomaterials*, **271**, 120739. https://doi.org/10.1016/j.biomaterials.2021.1.

Yusoff, A.H., Salimi, M.N. and Jamlos, M.F. (2018), "A review: Synthetic strategy control of magnetite nanoparticles production", *Adv. Nano Res.*, **6(1)**, 1-19. https://doi.org/10.12989/anr.2018.6.1.001.

Zhao, J., Huggins, F.E., Feng, Z. and Huffman, G.P. (1996), "Surface-induced superparamagnetic relaxation in nanoscale ferrihydrite particles", *Phys. Rev. B*, **54**(5), 3403-3407. https://doi.org/10.1103/physrevb.54.3403.

*JL*